Engineering 4 (2018) 779–786

Contents lists available at ScienceDirect

Engineering

journal homepage: www.elsevier.com/locate/eng

Research
Precision Engineering—Review

# Ultra-Short Pulsed Laser Manufacturing and Surface Processing of Microdevices

Yongchao Yu [a], Shi Bai [b], Shutong Wang [c], Anming Hu [a,b,*]

[a] Department of Mechanical, Aerospace and Biomedical Engineering, University of Tennessee, Knoxville, TN 37996, USA
[b] Institute of Laser Engineering, Beijing University of Technology, Beijing 100124, China
[c] College of Electronics and Information Engineering, Sichuan University, Chengdu 610064, China

ARTICLE INFO

*Article history:*
Received 28 April 2018
Revised 21 August 2018
Accepted 25 October 2018
Available online 1 November 2018

*Keywords:*
Ultra-short pulsed laser processing
Microdevices
Supercapacitor
Electronic tongue
Surface-enhanced Raman spectroscopy

ABSTRACT

Ultra-short laser pulses possess many advantages for materials processing. Ultrafast laser has a significantly low thermal effect on the areas surrounding the focal point; therefore, it is a promising tool for micro- and submicro-sized precision processing. In addition, the nonlinear multiphoton absorption phenomenon of focused ultra-short pulses provides a promising method for the fabrication of various structures on transparent material, such as glass and transparent polymers. A laser direct writing process was applied in the fabrication of high-performance three-dimensional (3D) structured multilayer micro-supercapacitors (MSCs) on polymer substrates exhibiting a peak specific capacitance of 42.6 mF·cm$^{-2}$ at a current density of 0.1 mA·cm$^{-2}$. Furthermore, a flexible smart sensor array on a polymer substrate was fabricated for multi-flavor detection. Different surface treatments such as gold plating, reduced-graphene oxide (rGO) coating, and polyaniline (PANI) coating were accomplished for different measurement units. By applying principal component analysis (PCA), this sensing system showed a promising result for flavor detection. In addition, two-dimensional (2D) periodic metal nanostructures inside 3D glass microfluidic channels were developed by all-femtosecond-laser processing for real-time surface-enhanced Raman spectroscopy (SERS). The processing mechanisms included laser ablation, laser reduction, and laser-induced surface nano-engineering. These works demonstrate the attractive potential of ultra-short pulsed laser for surface precision manufacturing.



## 1. Introduction

The use of ultrafast lasers, which emit light pulses with a period shorter than a nanosecond, for material processes was first reported in 1987 by Srinivasan et al. [1] and Küper and Stuke [2]. That study demonstrated that with the use of a femtosecond ultraviolet excimer laser, polymethyl methacrylate could be ablated without the formation of a heat-affected zone. In comparison with nanosecond laser ablation, the ablation threshold for ultrafast lasers is significantly lower. Limited heating diffusion in the surrounding region of the processed area is an important feature of ultrafast laser processing [3,4], as it allows high-precision microfabrication with various materials, such as biological tissues, semiconductors, and insulators [5]. During an ultrafast interaction, the absorption of photons stimulates the carriers within a hundred femtoseconds, which is too short of a time period to disturb the lattice. Efficient energy transfer from the electrons to the lattice thus occurs by electron-lattice scattering at the end of the laser pulse [6,7]. Depending on the electron–phonon coupling strength of different materials, the thermal coupling between free electrons and lattices typically occurs in the range of 1–100 ps. The typical electron–phonon coupling time of a hundred femtoseconds is much shorter than the heat-transfer period by thermal conduction. Therefore, thermal diffusion to the laser-irradiated surrounding area is very limited [8], which is a very attractive feature of high-resolution ultrafast laser processing. In an ideal case, ultrafast excitation only occurs within the focal spot. However, for a laser pulse with a duration of a few picoseconds or longer, thermal diffusion cannot be neglected.

Nonlinear multiphoton absorption is another important aspect of ultrafast laser processing. The probability of multiphoton absorption can be significantly increased by the extremely high

* Corresponding author.
*E-mail address:* ahu3@utk.edu (A. Hu).

https://doi.org/10.1016/j.eng.2018.10.004

laser peak intensity of tightly focused ultra-short laser pulses, since the probability is a power function of the peak intensity [9,10]. The highly localized nonlinear effect of an ultra-short laser leads to super-resolution processing beyond the optical diffraction limit; strong absorption can even occur in a transparent material [5,7,11–13]. The multiphoton absorption phenomenon that generated by ultrafast laser not only permits surface processing, but also permits internal microfabrication of transparent materials such as glass and polymer. This paper mainly reviews three works covering the following topics: high-performance micro-supercapacitors (MSCs) fabricated by a femtosecond three-dimensional (3D) laser direct writing process, flexible smart sensor arrays on polymer substrates for multi-flavor detection, and all-femtosecond-laser-processing microfluidic surface-enhanced Raman spectroscopy (SERS) chips fabrication.

## 2. Laser direct writing on polymer substrates for energy device and sensor applications

### 2.1. High-performance MSC fabricated by 3D laser direct writing

The laser ablation of polymeric materials has been studied since 1980 [14]. Since then, numerous applications have been reported, especially in the field of optics [15–19]. In 2014, Lin et al. [14] reported their research on laser-induced graphene (LIG) films from commercial polyimide (PI). The C—O, C═O, and N—C bonds contained in the PI film were easily broken by means of laser irradiation, and were then rearranged to form porous structures. An interdigitated LIG MSC with an areal capacitance of 4 $mF{\cdot}cm^{-2}$ at 20 $mV{\cdot}s^{-1}$ was fabricated in that study. LIG has a relatively large surface ratio, as well as a porous structure with good conductivity. Thus, laser direct writing on polymer substrates has become a very promising process for fixable electrical devices, such as sensors, medical devices, communication devices, optical devices, and energy-storage devices [18,20–27]. In et al. [24] demonstrated a flexible supercapacitor with a specific capacitance of about 800 $\mu F{\cdot}cm^{-2}$ at a 10 $mV{\cdot}s^{-1}$ scan rate, based on femtosecond laser-induced porous carbon on a PI substrate. Li et al. [28] developed the laser direct writing of graphene oxide (rGO) with gold (Au) nanocomposite MSCs with an areal capacitance of 0.46 $mF{\cdot}cm^{-2}$ at a high scan rate of 100 $V{\cdot}s^{-1}$. Cai et al. [26] utilized a 405 nm semiconductor laser to irradiate a PI sheet in order to prepare the carbon electrodes (CEs) of supercapacitors. The obtained supercapacitors exhibited a high performance of about 31.9 $mF{\cdot}cm^{-2}$ at a current density of 0.05 $mA{\cdot}cm^{-2}$, as a result of the hierarchical porous structures and thick CEs that were formed during the laser writing process.

Wang et al. [29] reported a novel fabrication process in which a 3D laser direct writing technique was used to fabricate multilayer MSCs via a bottom-to-top process on a PI substrate. Fig. 1(a) shows a scanning electron microscope (SEM) image for the cross-section of the three-layer (3L) MSCs. In order to realize a stable interconnection, the conductive layers were partially overlapped with a total thickness of around 140 μm for the 3L MSCs. First, the femtosecond laser was focused at a position 80 μm below the surface of the PI sheets by a 50× objective lens to induce the carbonization of the bottom layer. The second carbonization layer was then written by the focused laser at a position 65 μm below the surface of the PI sheets, thus creating the middle layer. Finally, the focusing laser was adjusted to the surface of the PI sheets in order to realize surface carbonization. After the laser writing, the carbonized electrode was treated with plasma for 5 min in order to change the wetting property from hydrophobic to hydrophilic. This process results in more contact area between the electrolyte and the CEs; it also helps with the permeation of the electrolyte. Next, polyvinyl alcohol-sulfuric acid (PVA-$H_2SO_4$) was applied to the electrodes as the electrolyte for the measurement of the capacitor performance. Before the measurements were taken, the MSCs were left at room temperature overnight in order to dry the electrolyte completely. Fig. 1(b) presents the specific capacitance values of one-layer (1L), two-layer (2L), and 3L MSCs at different current densities, as calculated from the galvanostatic charge/discharge (GCD) curves. In particular, the 3L stacked MSCs show a specific capacitance as high as 42.6 $mF{\cdot}cm^{-2}$ at a current density of 0.1 $mA{\cdot}cm^{-2}$, which is much higher than the 2L MSCs that have been reported elsewhere [14,24,26]. This improved capacity can be attributed to the porous thick electrode and to the nitrogen (N) atoms that partially replace the carbon (C) atoms in the graphitic carbon framework.

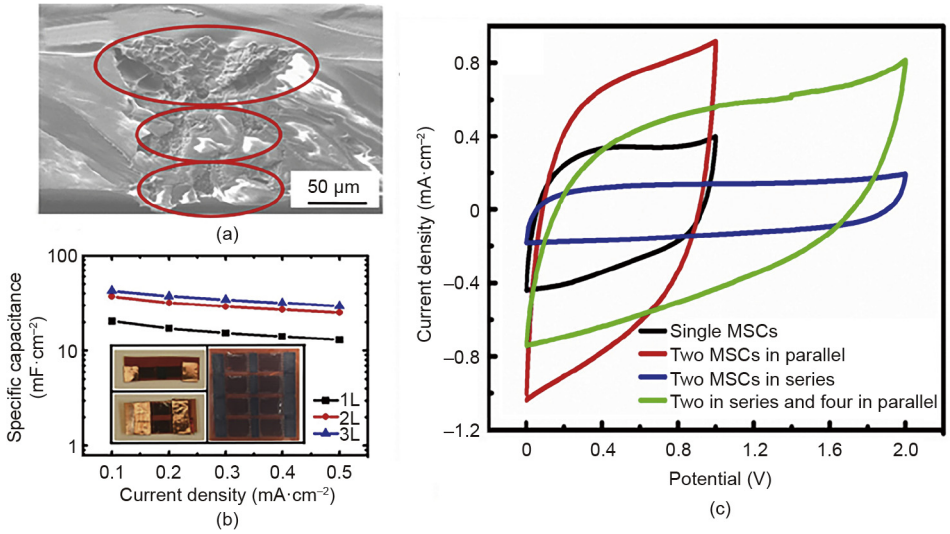


**Fig. 1.** (a) Cross-section of the 3L electrode. (b) Specific capacitances of the MSCs calculated from the GCD curves as a function of the current density. Photos of the fabricated (CEs) with different connections are inserted at the bottom of the figure. (c) GCD curves of MSCs with four kinds of connections at a current density of 0.1 $mA{\cdot}cm^{-2}$. (Reproduced from Ref. [29])

Moreover, in order to increase the operating voltages and currents of the MSCs, series-parallel connected MSCs were created using laser direct writing technology. Fig. 1(b) contains inserted images showing different MSCs connected in parallel, series, or combination on a single PI substrate. Fig. 1(c) displays the cyclic voltammetry curves for different connections of MSCs at a scan rate of 10 $mV \cdot s^{-1}$. Compared with a single MSC, two parallel connected MSCs give a double output current (red curve). Two series connected MSCs enlarge the voltage window from 1 to 2 V (blue curve), while the output current declines to half of that of the single MSC. A 2 × 4-combination connected MSC can double the voltage and output current (green curve). These results indicate that an MSC with diverse connections can meet the demands of different working voltages and currents. Due to the superior performance of carbon-based MSCs, femtosecond laser direct writing technology is an effective and advanced manufacturing technology for on-chip energy-storage devices. Furthermore, 3D laser direct writing has been developed not only to fabricate multilayer supercapacitors, but also to fabricate field-effect transistors, which will become a significant benefit for biosensor and certain power applications [30,31].

### 2.2. A multi-flavor detection flexible smart sensor array fabricated by femtosecond laser direct writing

Biosensors are another promising application for laser-induced porous graphene [21,32]. Bio-nanosensing technology has been developed for biomedical diagnostics [33]; environmental pollution monitoring [21,34]; and the measurement of temperature [35], humidity, and other physical parameters [36–39]. The general drawback of these sensors is that they are specifically designed for a particular objective. Porous carbon structures with a very high surface-to-volume ratio can be functionalized with an aptamer for specific sensing. However, for a pristine sensor without an aptamer coating, the sensor presents a very limited selectivity and is considered to be nonselective.

The concept of an electronic nose was first reported by Persaud and Dodd in 1982 [40]. An array of chemical sensors was used to simulate receptors and neural analysis in order to recognize a pattern of stimulations through pattern-recognition methods [40]. The name "electronic tongue" was presented in 1985 by Otto and Thomas [41], who demonstrated a liquid analysis system based on a multisensory array. The development of a multi-array sensing system underwent further rapid progress in the early 2000s. Although many sensing techniques have been developed for electronic tongue application, including optical and enzymatic sensors [42–44], the electrochemical or voltammetric-based sensor is still one of the most widely used sensing techniques [45].

Promising results have recently been demonstrated for biosensing using a sensor array for multi-element detection. Facure et al. [46] reported a novel electronic tongue system for the detection of organophosphate pesticides. Their sensing system contained four gold-electrode sensing units, which were functionalized with rGO or Au nano-particles, respectively. The sensing system successfully detected cadusafos and malathion at concentrations as low as 0.1 $mmoL \cdot L^{-1}$. Zhao et al. [47] reported an e-nose sensing array for the detection of volatile organic compounds (VOCs). Each VOC element was carried by nitrogen ($N_2$) gas and delivered to the sensing setup, with the concentration of the VOCs being controlled by the pressure ratio of $N_2$ gas and VOC vapor. Seven targeted compounds—ethanol, isopropyl alcohol (IPA), acetone, methanol, hexane, cyclohexane, and heptane—were detected by seven sensing units with a concentration range of $P/P_0$ from 0.1 to 0.8, where $P$ stands for the partial pressure and $P_0$ stands for the saturated vapor pressure of the VOCs at room temperature. It is notable that most of these sensing array systems were fabricated using a cleanroom technology, which is more complicated than the laser direct writing presented in this paper.

Here, we report on our recent work with a flexible sensor array fabricated by femtosecond laser direct writing for multi-flavor detection [48]. A femtosecond laser with a wavelength of 1030 nm was used as the laser source, and the laser was focused onto the surface of a PI substrate. During laser irradiation, the substrate was carried by a 3D programmable stage in order to create different pre-programmed patterns. For this experiment, CEs were fabricated at a laser power of 600 mW with a writing speed of 60 $mm \cdot min^{-1}$. Fig. 2(a) shows the fabricated CEs on a PI substrate, which is presented as a single measurement unit in this study. Fig. 2(b) displays a sensor array with six sensing units. Integrating the responses from different measurement units into a single sensor array implements cross-sensitivity; as a result, the system responds to different analytes without functionalization with probe molecules for specific analytes [49]. In order to enhance the selectivity and sensitivity of a sensor system, it is considered ideal to have a significant response difference between two measurement units corresponding to the same analyte. Six different types of sensor units were prepared by different surface treatments on CEs in order to achieve electronic tongue-style sensing.

For sensor functionalization, different surface treatments were performed on the laser-induced CEs surface. Six different electrodes constituted a sensor array for the measurement, as follows: a CE gold-plated carbon electrode (GCE), rGO drop-coated carbon electrode (rGO-CE), rGO drop-coated gold-plated carbon electrode (rGO-GCE), polyaniline-deposited carbon electrode (PANI-CE), and polyaniline-deposited gold-plated carbon electrode (PANI-GCE). Fig. 3(a–f) provides typical SEM images of the surface structures for each electrode sample.

As shown in Fig. 4, the separation and grouping of datasets were observed after principal component analysis (PCA). In addition, linear dependencies were observed with changes in sample concentration. The sodium chloride (NaCl) samples are grouped at the mid-left side of the plot. As the concentration of NaCl decreases, the data points move to the right, and some changes occur in the vertical direction. The vinegar samples show a very clear linear dependence as the samples are diluted from 100% to 1%. The data points move from the left side to the right side of the plot and gradually rise. Furthermore, a clear linear dependency can be observed for the sugar samples, with the data points being grouped on the right side of the plot. With a decrease in concentration, the dataset moves to the top. This PCA graph demonstrates that this sensor array system can determine different targets—in this case, NaCl, vinegar, and sugar. By grouping the data points and mapping them on the graph, the sensor array system can be used to differentiate between NaCl, vinegar, and sugar solutions.

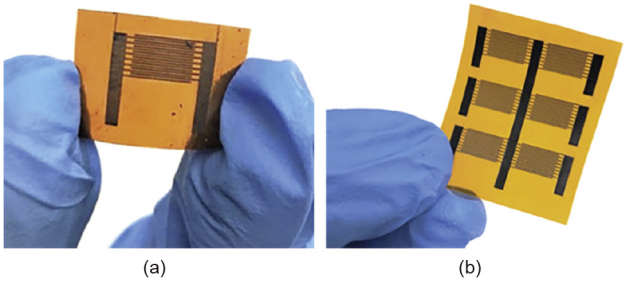


**Fig. 2.** (a) A fabricated CE; (b) a fabricated sensor array. (Reproduced from Ref. [48])

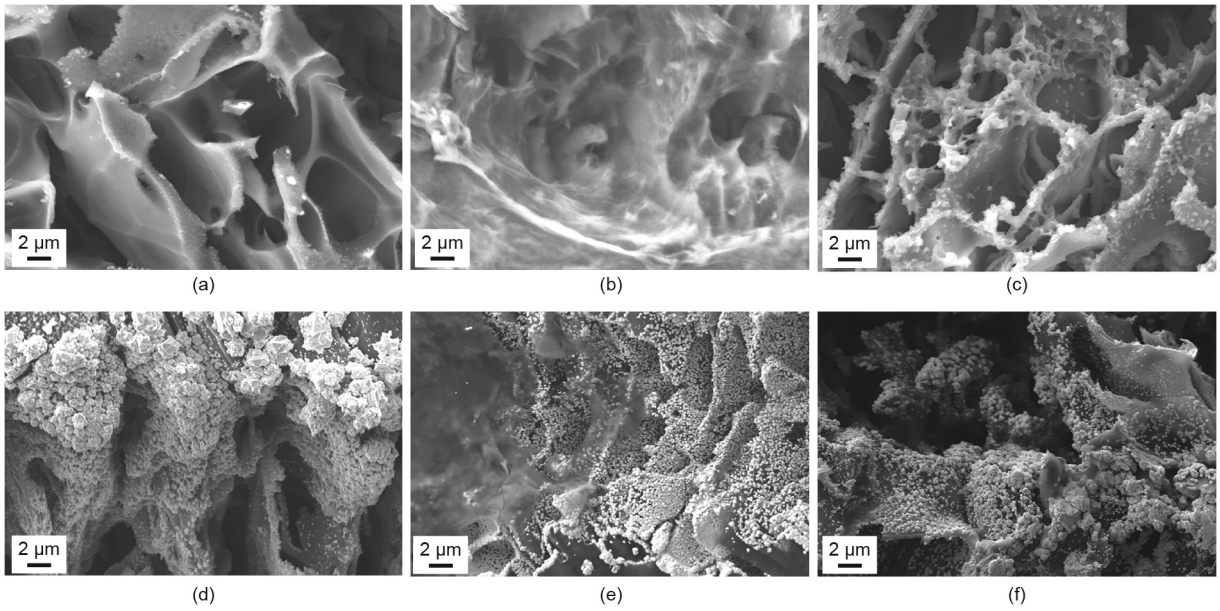


**Fig. 3.** SEM images of (a) CE; (b) rGO-CE; (c) PANI-CE; (d) GCE; (e) rGO-GCE; (f) PANI-GCE. (Reproduced from Ref. [48])

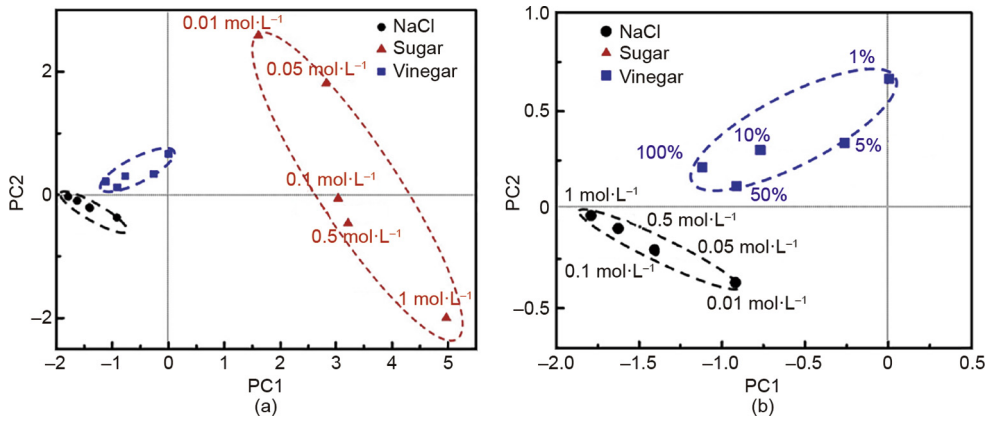


**Fig. 4.** Principal component factor scores obtained for target solutions. PC1 and PC2 represent the directions in which the data show the largest and second largest variations. (Reproduced from Ref. [48])

## 3. Microfluidic SERS chips fabricated by all-femtosecond-laser processing

SERS has a superior ability to detect analytes adsorbed on the surface of nano-sized metal structures with extremely low concentration in the analysis of various material [50–52], chemical [53,54], biological [55,56], and environmental specimens [57,58]. The enhanced Raman scattering of molecules adsorbed on rough metal surfaces [59] is a result of localized surface plasmon resonance (LSPR) [60], in which an enormous optical near-field enhancement is motivated by the excitation of a collective electron oscillation [61]. Experiments show that the enhancement factors are in the range of $10^6$–$10^8$ [62]. The electromagnetic field intensity on a SERS substrate is further determined by the surface geometries of the metal nanostructures, including shape, size, and layout [50,61,63]. In 2016, Lin et al. [64] reported on a SERS system with hexagonal-packed silicon nanorod (SiNR) arrays coated with Au nanoparticles. This SERS system provided an enhancement factor of $1 \times 10^7$ with a standard deviation of 3.9%–7.2% for detecting Rhodamine 6G (R6G) molecules. By employing unique femtosecond laser-metal interaction, it is possible to fabricate highly sensitive plasmonic substrates for SERS application. In 2014, Yang et al. [65] reported a SERS application using microgrooves on Si substrates. These grooves were directly created on a Si substrate by laser ablation. With the deposition of silver (Ag) film, the SERS chip exhibited an enhancement factor of $5.5 \times 10^6$ at an excitation wavelength of 532 nm. Recently, Bai et al. [66] developed a SERS device with an enhancement of $1 \times 10^8$ and a relative standard deviation of 8.8%. The SERS chip was fabricated by all-femtosecond-laser processing with no bonding procedures and no lithography for both micro and nanostructuring on glass substrates.

It has long been known that it is very challenging to fabricate a 3D metallic nanostructure (height > 1 μm) in a closed space with controlled patterns, since the nanostructure must be generated in the expected area and then grow into the desired sizes and shapes. In Bai's recently reported method [66], the linear patterns are first generated by laser-induced periodic surface structures (LIPSSs). The orientation of the LIPSS is parallel to the laser polarized direction. Next, the surface is irradiated again with the laser after the

polarization direction has been rotated by 90°. The two sets of orthorhombic LIPPS can form pseudo-ordered nanorod arrays for highly sensitive SERS. Online real-time SERS monitoring has been successfully realized with the use of such a microfluidic SERS chip [56].

The fabrication process is roughly divided into three steps: first, microchannel fabrication in a glass substrate by femtosecond laser direct patterning and laser-assisted wet etching; second, laser selective metallization of the copper (Cu)–Ag layered thin film inside the microchannel; and third, formation of a 2D periodic metal nanostructure by means of a femtosecond laser-induced periodic surface structure. Fig. 5 illustrates these process steps [66].

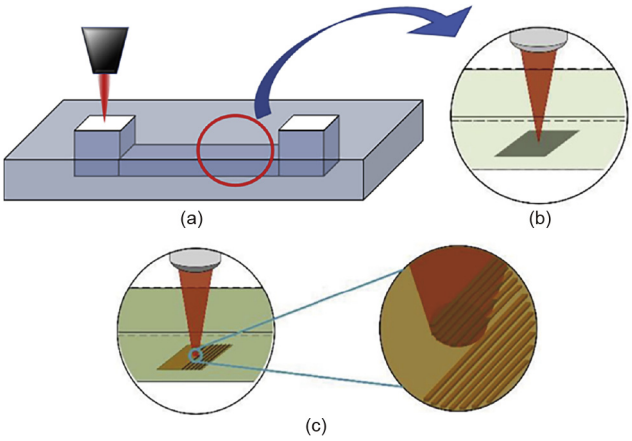


**Fig. 5.** The procedure used to fabricate a 3D microfluidic SERS chip by all-femtosecond-laser processing. (a) Femtosecond laser-assisted wet etching; (b) femtosecond laser selective metallization; (c) laser-induced periodic surface structure. (Reproduced form Ref. [66])

Fig. 6 shows the microstructure details of the SERS chip [66]. A microchannel was embedded in a glass substrate by femtosecond laser-assisted wet etching, as shown in Fig. 6(a). A femtosecond laser with a pulse duration of 457 fs, a central wavelength of 1045 nm, and a repetition rate of 100 kHz was employed for the direct patterning and etching process in order to obtain 3D microchannels in glass. The laser power and scanning speed were set to 25 mW and 1.5 $mm \cdot s^{-1}$, respectively. An extremely smooth surface with a nanoscale roughness was obtained after thermal annealing of the glass substrate. Fig. 6(b) shows an image of the inside wall of the microchannel modified by femtosecond laser ablation in water. The laser power was set at about 80 mW during irradiation. Obvious jagged grooves were created in the ablated area. The size of the ablation area was 30 μm × 30 μm with a line width of 5 μm, and the final roughness was increased to 0.3 μm. A Cu–Ag layer film was then deposited on the ablated area through the electroless plating of first Cu and then Ag by means of a galvanic displacement process. The mixing of Cu and Ag was intended to optimize the microstructures and SERS enhancement. Fig. 6(c) shows an SEM image of the surface morphologies of the deposited Cu–Ag film. The size of the grains ranged from 6 to 10 μm, and the film had an approximate thickness of 600 nm. In order to reduce the thickness of the film and the roughness, polyvinyl pyrrolidine (PVP) was added to the plating solution. This allowed the film thickness to be reduced to around 400 nm.

Fig. 7 shows SEM images of the periodic metal nanostructures that were fabricated by means of a femtosecond laser [66]. No surface nanostructures were formed at a laser power lower than 20 mW. When the laser power was increased, a 250 nm nanograting formed at a laser power of 30 mW, as shown in Fig. 7(a). However, when the laser power was increased further to 50 mW, laser irradiation did not produce a high spatial-frequency periodic surface structure (HSFL); instead, it deposited a large amount of devoirs, which covered most of the surface (Fig. 7(b)). Through a

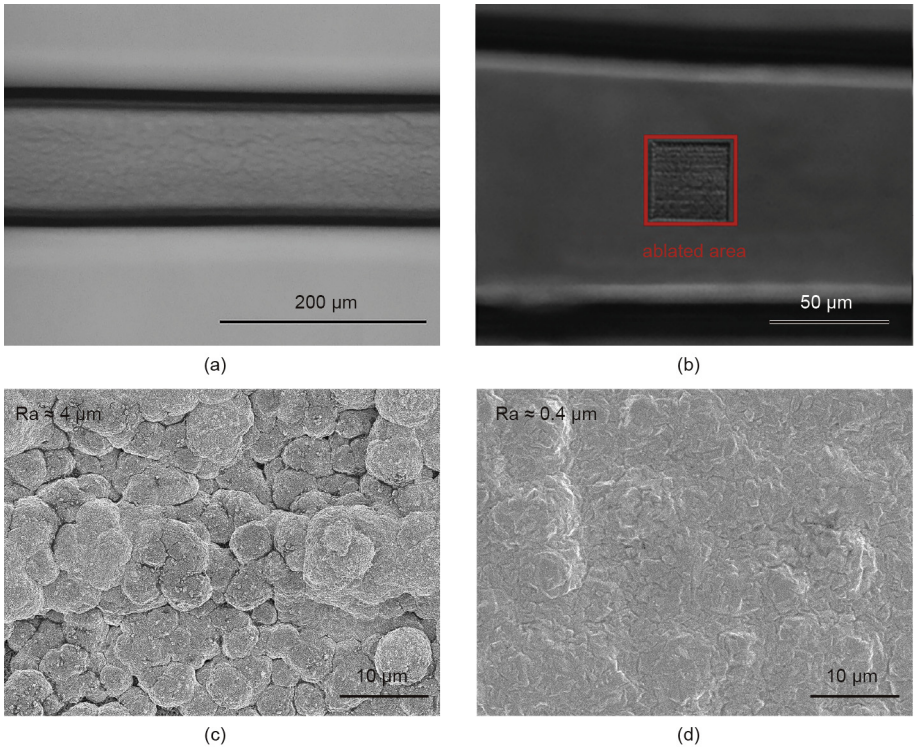


**Fig. 6.** Optical micrographs of (a) the microchannel embedded in the glass substrate; and (b) the femtosecond laser-ablated area on the bottom surface of the closed glass microchannel. The bottom parts of the figure show SEM images of the Cu film morphology obtained (c) without and (d) with polyvinyl pyrrolidine (PVP). (Reproduced from Ref. [66])

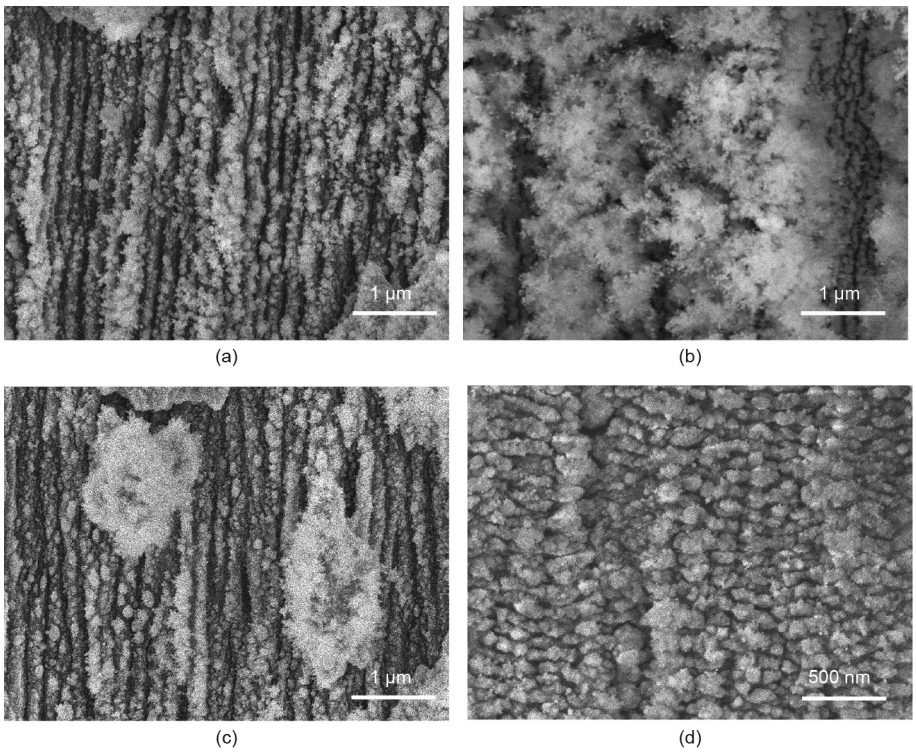


**Fig. 7.** SEM micrographs of the periodic metal nanostructures fabricated by irradiation with a linearly polarized femtosecond laser at a scanning speed of 1.5 mm·s$^{-1}$ and laser power levels of (a) 30 mW and (b) 50 mW; and at a laser power level of 30 mW and a scanning speed of (c) 0.25 mm·s$^{-1}$ and (d) 1.5 mm·s$^{-1}$. (Reproduced from Ref. [66])

comparison with multiple experimental results, 30 mW was determined to be an appropriate laser power. The laser scanning speed was similarly determined through a number of attempts. At a low scanning speed (0.25 mm·s$^{-1}$), an HSFL with a clear grid pattern was formed; however, due to a large amount of material being removed, plenty of debris was deposited on the surface (Fig. 7(c)). On the other hand, at a high scanning speed, the grain size distribution became wider. In subsequent trials, a scanning speed of 1.5 mm·s$^{-1}$ and a laser power of 30 mW were employed in order to optimize the nanostructures. Fig. 7(d) shows a clear 2D nanodot array with an average width of 200 nm and a height of 250 nm; this was created by femtosecond laser nanoengineering with the aforementioned parameters.

Fig. 8(a) presents the Raman spectra of R6G solutions at concentrations ranging from $10^{-5}$ to $10^{-9}$ mol·L$^{-1}$. The Raman peaks gradually decrease as the concentration of R6G decreases. When the concentration is lower than $10^{-9}$ mol·L$^{-1}$, the Raman peaks became hardly observable, which illustrates the detection limit of $10^{-9}$ mol·L$^{-1}$ for R6G detection. The inset of Fig. 8(a) repents the Raman spectrum of $10^{-2}$ mol·L$^{-1}$ R6G on flat glass enlarged five times. A comparison of these two graphs reveals a very considerable enforcement of the Raman spectrum for the SERS chip. Fig. 8(b) shows the results from the real-time SERS sensing of cadmium ion ($Cd^{2+}$) solutions with varied concentrations. When $Cd^{2+}$ solutions with different concentrations were injected into the microchannel, intensity changes in the SERS were observed as a

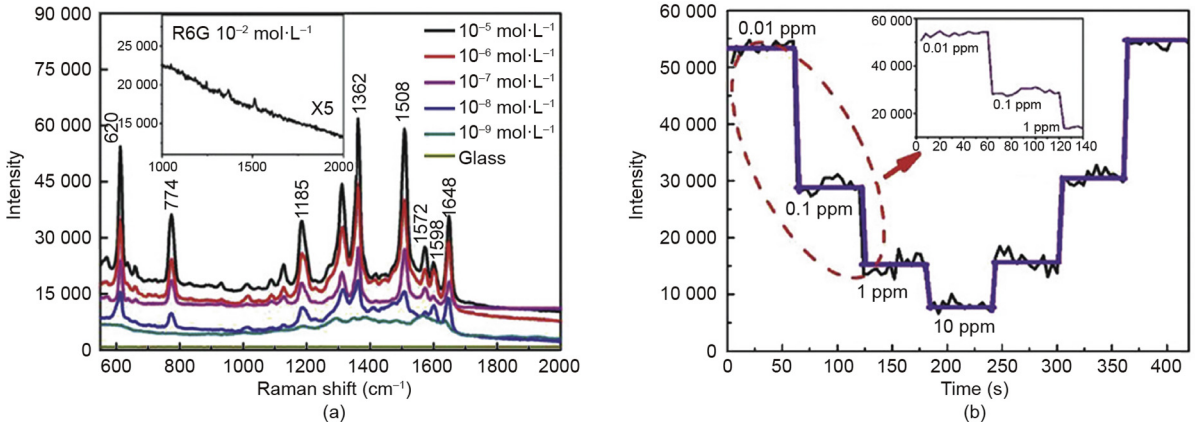


**Fig. 8.** (a) SERS spectra of R6G solutions with varying concentrations on the 2D periodic Cu–Ag nanostructured SERS substrate, where the yellow line corresponds to the spectrum of the Fortuna glass. The inset shows the Raman spectrum of $10^{-2}$ moL·L$^{-1}$ R6G on flat glass enlarged five times. (b) The intensity of the $10^{-5}$ mol·L$^{-1}$ CV Raman peak over time while injecting $Cd^{2+}$ solutions with various concentrations. The inset shows a magnified image of the region circled with a red dashed line from 0.01 to 1 ppm. (Reproduced from Ref. [66])

function of solution concentration over time. Each solution was injected over a period of 1.5 min with a flow rate of 10 μL·min$^{-1}$, and the spectra were recorded for 10 s.

In a further reduction of the detection limit, Yang et al. [67] reported a SERS platform based on slippery liquid-infused porous surfaces (SLIPS) inspired by the pitcher plant. This superhydrophobic slippery substrate was created by dipping a nano-textured surface into a perfluorinated liquid. In the experiment, ethanol was selected to represent a non-aqueous liquid. R6G was selected as a target element in order to demonstrate the detection limit. Au nanoparticles were added to the solution to create "hotspots" for SERS measurements. For the measurements, 50 μL of R6G ethanol solutions with different concentrations of R6G were dropped onto the platform surface. After the ethanol fully evaporated, a close-packed R6G/Au aggregate of approximately 150 μm in diameter formed, which was used for the SERS detection. The results showed that 750 mol·L$^{-1}$ of the R6G molecule was detected with over 90% systematically quantified probability, and a minimum of 75 mol·L$^{-1}$ with 1.4% probability. Thus, with the further development of laser precision machining, it is possible to produce bio-inspired nanostructures for SERS measurements.

## 4. Conclusions

In this paper, three works involving the precise laser processing of a multilayer supercapacitor array, a smart sensor array, and microfluidic chips for SERS analysis were reported on and discussed in detail. The microscale devices were fabricated on transparent polymeric materials and glass substrates. These works demonstrate that material properties and microstructures can be controlled by means of an ultrafast laser, with suppression of thermal diffusion. High-resolution fabrication with various materials using focused ultra-short laser pulses has been demonstrated for high energy-density storage and super-sensitive sensing. These 3D structured micro-/nano-scale components and devices thus demonstrate successful laser precision manufacturing for optical, electrical, and lab-on-a-chip applications.

## Acknowledgements

We appreciated a technical maturation grant provided by the University of Tennessee Research Foundation and a grant from the National Natural Science Foundation of China (51575016). The Fundamental Research Funds for the Central Universities also supported this work. Wang and Bai gratefully acknowledge financial support from the China Scholarship Council.

## Compliance with ethics guidelines

Yongchao Yu, Shi Bai, Shutong Wang, and Anming Hu declare that they have no conflict of interest or financial conflicts to disclose.

## References

[1] Srinivasan R, Sutcliffe E, Braren B. Ablation and etching of polymethylmethacrylate by very short (160 fs) ultraviolet (308 nm) laser pulses. Appl Phys Lett 1987;51(16):1285–7.
[2] Küper S, Stuke M. Femtosecond UV excimer laser ablation. Appl Phys B 1987;44(4):199–204.
[3] Yanik MF, Cinar H, Cinar HN, Chisholm AD, Jin Y, Ben-Yakar A. Functional regeneration after laser axotomy. Nature 2004;432(7019):822.
[4] Momma C, Chichkov BN, Nolte S, Von Alvensleben F, Tünnermann A, Welling H, et al. Short-pulse laser ablation of solid targets. Opt Commun 1996;129(1–2):134–42.
[5] Bärsch N, Körber K, Ostendorf A, Tönshoff KH. Ablation and cutting of planar silicon devices using femtosecond laser pulses. Appl Phys A 2003;77(2):237–42.
[6] Wellershoff SS, Hohlfeld J, Güdde J, Matthias E. The role of electron–phonon coupling in femtosecond laser damage of metals. Appl Phys A 1999;69(1):S99–107.
[7] Gattass RR, Mazur E. Femtosecond laser micromachining in transparent materials. Nat Photonics 2008;2(4):219–25.
[8] Sugioka K, Cheng Y. Ultrafast lasers—reliable tools for advanced materials processing. Light Sci Appl 2014;3(4):e149.
[9] Hu A, Rybachuk M, Lu QB, Duley WW. Direct synthesis of sp-bonded carbon chains on graphite surface by femtosecond laser irradiation. Appl Phys Lett 2007;91(13):131906.
[10] Zheng C, Hu A, Chen T, Oakes KD, Liu S. Femtosecond laser internal manufacturing of three-dimensional microstructure devices. Appl Phys A 2015;121(1):163–77.
[11] Fischer J, Wegener M. Three-dimensional optical laser lithography beyond the diffraction limit. Laser Photonics Rev 2013;7(1):22–44.
[12] Zhou W, Bridges D, Li R, Bai S, Ma Y, Hou T, et al. Recent progress of laser micro- and nano-manufacturing. Sci Lett J 2016;5:228.
[13] Küper S, Stuke M. Ablation of UV-transparent materials with femtosecond UV excimer laser pulses. Microelectro Eng 1989;9(1–4):475–80.
[14] Lin J, Peng Z, Liu Y, Ruiz-Zepeda F, Ye R, Samuel ELG, et al. Laser-induced porous graphene films from commercial polymers. Nat Commun 2014;5(1):5714.
[15] Watanabe W, Sowa S, Tamaki T, Itoh K, Nishii J. Three-dimensional waveguides fabricated in poly(methyl methacrylate) by a femtosecond laser. Jpn J Appl Phys 2006;45(29):L765–7.
[16] Yamasaki K, Juodkazis S, Watanabe M, Sun HB, Matsuo S, Misawa H. Recording by microexplosion and two-photon reading of three-dimensional optical memory in polymethylmethacrylate films. Appl Phys Lett 2000;76(8):1000–2.
[17] Sowa S, Watanabe W, Tamaki T, Nishii J, Itoh K. Symmetric waveguides in poly (methyl methacrylate) fabricated by femtosecond laser pulses. Opt Express 2006;14(1):291–7.
[18] Zheng C, Hu A, Li R, Bridges D, Chen T. Fabrication of embedded microball lens in PMMA with high repetition rate femtosecond fiber laser. Opt Express 2015;23(13):17584–98.
[19] Zheng C, Hu A, Kihm KD, Ma Q, Li R, Chen T, et al. Femtosecond laser fabrication of cavity microball lens (CMBL) inside a PMMA substrate for super-wide angle imaging. Small 2015;11(25):3007–16.
[20] Beidaghi M, Wang C. Micro-supercapacitors based on interdigital electrodes of reduced graphene oxide and carbon nanotube composites with ultrahigh power handling performance. Adv Funct Mater 2012;22(21):4501–10.
[21] Cheng C, Wang S, Wu J, Yu Y, Li R, Eda S, et al. Bisphenol a sensors on polyimide fabricated by laser direct writing for onsite river water monitoring at attomolar concentration. ACS Appl Mater Interfaces 2016;8(28):17784–92.
[22] Deubel M, Von Freymann G, Wegener M, Pereira S, Busch K, Soukoulis CM. Direct laser writing of three-dimensional photonic-crystal templates for telecommunications. Nat Mater 2004;3(7):444–7.
[23] Gittard SD, Narayan RJ. Laser direct writing of micro- and nano-scale medical devices. Expert Rev Med Devices 2010;7(3):343–56.
[24] In JB, Hsia B, Yoo JH, Hyun S, Carraro C, Maboudian R, et al. Facile fabrication of flexible all solid-state micro-supercapacitor by direct laser writing of porous carbon in polyimide. Carbon 2015;83:144–51.
[25] Luo S, Hoang PT, Liu T. Direct laser writing for creating porous graphitic structures and their use for flexible and highly sensitive sensor and sensor arrays. Carbon 2016;96:522–31.
[26] Cai J, Lv C, Watanabe A. Cost-effective fabrication of high-performance flexible all-solid-state carbon micro-supercapacitors by blue-violet laser direct writing and further surface treatment. J Mater Chem A Mater Energy Sustain 2016;4(5):1671–9.
[27] Hou T, Zheng C, Bai S, Ma Q, Bridges D, Hu A, et al. Fabrication, characterization, and applications of microlenses. Appl Opt 2015;54(24):7366–76.
[28] Li RZ, Peng R, Kihm KD, Bai S, Bridges D, Tumuluri U, et al. High-rate in-plane micro-supercapacitors scribed onto photo paper using in situ femtolaser-reduced graphene oxide/Au nanoparticle microelectrodes. Energy Environ Sci 2016;9(4):1458–67.
[29] Wang S, Yu Y, Li R, Feng G, Wu Z, Compagnini G, et al. High-performance stacked in-plane supercapacitors and supercapacitor array fabricated by femtosecond laser 3D direct writing on polyimide sheets. Electrochim Acta 2017;241:153–61.
[30] Tran TT, Mulchandani A. Carbon nanotubes and graphene nano field-effect transistor-based biosensors. TrAC Trends Analyt Chem 2016;79:222–32.
[31] Zhan B, Li C, Yang J, Huang W, Dong X. Graphene field-effect transistor and its application for electronic sensing. Small 2014;10(20):4042–65.
[32] Piqué A, Chrisey DB, Fitz-Gerald JM, McGill RA, Auyeung RCY, Wu HD, et al. Direct writing of electronic and sensor materials using a laser transfer technique. J Mater Res 2000;15(9):1872–5.
[33] Yu Y, Al Mamun KA, Shanta AS, Islam SK, McFarlane N. Vertically aligned carbon nanofibers as a cell impedance sensor. IEEE Trans NanoTechnol 2016;15(6):856–61.
[34] Malzahn K, Windmiller JR, Valdés-Ramírez G, Schöning MJ, Wang J. Wearable electrochemical sensors for *in situ* analysis in marine environments. Analyst 2011;136(14):2912–7.
[35] Bakker A, Huijsing JH. Micropower CMOS temperature sensor with digital output. IEEE J Solid-State Circuits 1996;31(7):933–7.
[36] Kuang Q, Lao C, Wang ZL, Xie Z, Zheng L. High-sensitivity humidity sensor based on a single $SnO_2$ nanowire. J Am Chem Soc 2007;129(19):6070–1.
[37] Sikarwar S, Yadav B. Opto-electronic humidity sensor: a review. Sens Actuators A Phys 2015;233:54–70.

[38] Mukhopadhyay SC. Wearable sensors for human activity monitoring: a review. IEEE Sens J 2015;15(3):1321–30.
[39] Li L, Zhang J, Peng Z, Li Y, Gao C, Ji Y, et al. High-performance pseudocapacitive microsupercapacitors from laser-induced graphene. Adv Mater 2016;28(5):838–45.
[40] Persaud K, Dodd G. Analysis of discrimination mechanisms in the mammalian olfactory system using a model nose. Nature 1982;299(5881):352–5.
[41] Otto M, Thomas J. Model studies on multiple channel analysis of free magnesium, calcium, sodium, and potassium at physiological concentration levels with ion-selective electrodes. Anal Chem 1985;57(13):2647–51.
[42] Premanode B, Toumazou C. A novel, low power biosensor for real time monitoring of creatinine and urea in peritoneal dialysis. Sens Actuators B 2007;120(2):732–5.
[43] Lvova L, Pudi R, Galloni P, Lippolis V, Di Natale C, Lundström I, et al. Multi-transduction sensing films for electronic tongue applications. Sens Actuators B 2015;207:1076–86.
[44] Gutés A, Ibáñez AB, Del Valle M, Céspedes F. Automated SIA e-tongue employing a voltammetric biosensor array for the simultaneous determination of glucose and ascorbic acid. Electroanalysis 2006;18(1):82–8.
[45] Ciosek P, Wroblewski W. Sensor arrays for liquid sensing—electronic tongue systems. Analyst 2007;132(10):963–78.
[46] Facure MH, Mercante LA, Mattoso LHC, Correa DS. Detection of trace levels of organophosphate pesticides using an electronic tongue based on graphene hybrid nanocomposites. Talanta 2017;167:59–66.
[47] Zhao Y, Yang Q, Chang Y, Qu H, Pang W, Zhang H, et al. Detection and discrimination of volatile organic compounds using a single multi-resonance mode piezotransduced silicon bulk acoustic wave resonator (PSBAR) as virtual sensor array. Sens Actuators B 2018;254:1191–9.
[48] Yu Y, Joshi PC, Wu J, Hu A. Laser-induced carbon base smart flexible sensor array for multi flavors detection. ACS Appl Mater Interfaces 2018 [Internet] [cited 2018 Sep 29]. Available from: https://pubs.acs.org/doi/abs/10.1021/acsami.8b12626.
[49] Riul Jr A, Dantas CAR, Miyazaki CM, Oliveira Jr ON. Recent advances in electronic tongues. Analyst 2010;135(10):2481–95.
[50] Bae Y, Kim NH, Kim M, Lee KY, Han SW. Anisotropic assembly of Ag nanoprisms. J Am Chem Soc 2008;130(16):5432–3.
[51] Hu A, Duley W. Surface enhanced Raman spectroscopic characterization of molecular structures in diamond-like carbon films. Chem Phys Lett 2008;450(4–6):375–8.
[52] Hu A, Lu QB, Duley WW, Rybachuk M. Spectroscopic characterization of carbon chains in nanostructured tetrahedral carbon films synthesized by femtosecond pulsed laser deposition. J Chem Phys 2007;126(15):154705.
[53] Phan-Quang GC, Wee EHZ, Yang F, Lee HK, Phang IY, Feng X, et al. Online flowing colloidosomes for sequential multi-analyte high-throughput SERS Analysis. Angew Chem Int Ed 2017;56(20):5565–9.
[54] Hu A, Sanderson J, Zaidi AA, Wang C, Zhang T, Zhou Y, et al. Direct synthesis of polyyne molecules in acetone by dissociation using femtosecond laser irradiation. Carbon 2008;46(13):1823–5.
[55] Pallaoro A, Hoonejani MR, Braun GB, Meinhart CD, Moskovits M. Rapid identification by surface-enhanced Raman spectroscopy of cancer cells at low concentrations flowing in a microfluidic channel. ACS Nano 2015;9(4):4328–36.
[56] Lu G, De Keersmaecker H, Su L, Kenens B, Rocha S, Fron E, et al. Live-cell SERS endoscopy using plasmonic nanowire waveguides. Adv Mater 2014;26(30):5124–8.
[57] Yin J, Wu T, Song J, Zhang Q, Liu S, Xu R, et al. SERS-active nanoparticles for sensitive and selective detection of cadmium ion ($Cd^{2+}$). Chem Mater 2011;23(21):4756–64.
[58] Bai S, Lin YH, Zhang XP, Zhou WP, Chen T, Ma Y, et al. Two-step photonic reduction of controlled periodic silver nanostructures for surface-enhanced Raman spectroscopy. Plasmonics 2015;10(6):1675–85.
[59] Blackie EJ, Le Ru EC, Etchegoin PG. Single-molecule surface-enhanced Raman spectroscopy of nonresonant molecules. J Am Chem Soc 2009;131(40):14466–72.
[60] Bai S, Zhou W, Tao C, Oakes K, Hu A. Laser-processed nanostructures of metallic substrates for surface-enhanced Raman spectroscopy. Curr Nanosci 2014;10(4):486–96.
[61] Zhang XY, Hu A, Zhang T, Lei W, Xue XJ, Zhou Y, et al. Self-assembly of large-scale and ultrathin silver nanoplate films with tunable plasmon resonance properties. ACS Nano 2011;5(11):9082–92.
[62] Kneipp K, Kneipp H, Manoharan R, Itzkan I, Dasari RR, Feld MS. Surface-enhanced Raman scattering (SERS)—a new tool for single molecule detection and identification. Bioimaging 1998;6(2):104–10.
[63] Bai S, Zhou W, Lin Y, Zhao Y, Chen T, Hu A, et al. Ultraviolet pulsed laser interference lithography and application of periodic structured Ag-nanoparticle films for surface-enhanced Raman spectroscopy. J Nanopart Res 2014;16(7):2470.
[64] Lin D, Wu Z, Li S, Zhao W, Ma C, Wang J, et al. Large-area Au-nanoparticle-functionalized Si nanorod arrays for spatially uniform surface-enhanced Raman spectroscopy. ACS Nano 2017;11(2):1478–87.
[65] Yang J, Li J, Du Z, Gong Q, Teng J, Hong M. Laser hybrid micro/nano-structuring of Si surfaces in air and its applications for SERS detection. Sci Rep 2014;4(1):6657.
[66] Bai S, Serien D, Hu A, Sugioka K. 3D microfluidic surface-enhanced raman spectroscopy (SERS) chips fabricated by all-femtosecond-laser-processing for real-time sensing of toxic substances. Adv Funct Mater 2018;28(23):1706262.
[67] Yang S, Dai X, Stogin BB, Wong TS. Ultrasensitive surface-enhanced Raman scattering detection in common fluids. Proc Natl Acad Sci USA 2016;113(2):268–73.